Journal of Alloys and Compounds 506 (2010) 317–322

Contents lists available at ScienceDirect

Journal of Alloys and Compounds

journal homepage: www.elsevier.com/locate/jallcom

Study on Si–Ti alloy dispersed in a glassy matrix as an anode material for lithium-ion batteries

Xiuyan Wang, Zhaoyin Wen*, Yu Liu, Lezhi Huang, Meifen Wu

CAS Key Laboratory of Materials for Energy Conversion, Shanghai Institute of Ceramics, Chinese Academy of Science, 1295 Dingxi Road, Shanghai 200050, PR China

ARTICLE INFO

Article history:
Received 23 January 2010
Received in revised form 28 June 2010
Accepted 30 June 2010
Available online 13 July 2010

Keywords:
Silicon-based anode
Si–Ti alloys
Glassy matrix
HEMM
Li-ion batteries

ABSTRACT

A nanosized silicon based composite consisting of Si, Si–Ti alloy phases dispersed in a glassy matrix is prepared by high energy mechanical milling (HEMM), followed by thermal treatment. X-ray diffraction (XRD), field emission scanning electron microscope (SEM) and transmission electron microscope (TEM) are used to determine the phases obtained and to observe the microstructure and distribution of the components. The galvanostatic discharge/charge test is carried out to characterize the electrochemical properties of the composite. The composite electrode delivered a reversible capacity of 738.6 mAh g^{-1} after 50 cycles and the coulombic efficiency remains above 95% from the 3rd cycle. When the discharge capacity is limited to 700 mAh g^{-1}, the reversible capacity is maintained at 675.8 mAh g^{-1} for 60 cycles without overcharge.

1. Introduction

Recently, with the development of portable devices and electric vehicles, lithium-ion batteries with high energy density and long-term cycle life have been given high demand. Silicon is one of the most promising candidates for the anode material of Li-ion batteries because of its largest theoretic capacity of 4008 mAh g^{-1} for the $Li_{22}Si_4$ alloy [1]. However, two major problems including the severe volume change upon alloying/dealloying process and the poor electrical conductivity seriously hinder its practical application. To solve these, lots of work has been done. Reducing the particle size of silicon is an effective way to minimize the absolute volume change [2,3]. However, the nanoparticles would aggregate to form inactive dense blocks during lithium insertion/extraction process thus a simple size reduction of the Si particles cannot effectively eliminate its capacity degradation. One effective way to improve the cyclability of silicon-based anode is synthesizing a composite structure by introducing buffering matrix which is electrochemically less active than Si or inactive and has good electrical conductivity. Carbonaceous materials, such as graphite and disordered carbon, have been investigated intensively as the buffering matrix for their good electronic conductivity, Li-insertion ability and small volume expansion [4–8]. Those Si/C composites have been found to show improved cyclability compared with Si. For instance, Datta and Kumta [4] prepared a series of Li–Si/C composite by terminating the electrochemical charging reaction of Li^+ following electrochemical activation of the Si/C composites generated by high energy mechanical milling (HEMM) at different potentials (~0.6, ~0.5 and ~0.4 V). The Li–Si/C composite synthesized at ~0.6 and ~0.5 V, cycled within their stable potential window, exhibit better cyclability than that of the pure Si/C composite electrode cycled in the potential window of 0.02–1.2 V. Gu et al. [8] synthesized a series of Si/C composites via high energy ball milling, followed by pyrolysis adopting citric acid as the carbon source. The as-prepared Si/C composite (5 h of ball milling followed by thermal treatment at 600 °C) electrode exhibited a discharge capacity of 626.7 mAh g^{-1} after 30 cycles, which is much better than the pure Si electrode. Zhou et al. [9] synthesized a kind of composite containing silicon (Si), disordered carbon (DC) and multi-walled carbon nanotubes (MWCNTs) by pyrolyzing the phenolformaldehyde resin (PFR) mixed with Si and MWCNTs, and a discharge capacity of 733 mAh g^{-1} was obtained after 20 cycles.

Another effective approach to overcome the detriment of Si anode is the use of Si-transition metal or Si–metal systems which have larger volumetric capacity than the Si–C composite, such as Si–Ni [10–12], Si–Cu [13–15], Si–Fe [16–18], Si–Ti [19,20], Al–Si–Mn [21], Si–Co–B–Al [22], Si–Co–Cr–Al–C [23], Si–$CeMg_2$ [24], and alloy systems. The silicon–transition metal alloy composites consist of active Si and Si–M alloy phases (M: Ni, Fe, Cu, Ti, Al, Co, Mn, Mg, etc.), in which nanosized Si particles are well distributed in the Si–M alloy phases. After the first lithium insertion/extraction process, a uniform composite structure with active silicon distributed in an inactive and conductive M matrix is formed, which could effectively alleviate the volume change and

* Corresponding author. Tel.: +86 21 52411704; fax: +86 21 52413903.
E-mail addresses: wangxiuyan021@163.com (X. Wang), zywen@mail.sic.ac.cn, xywang@mail.sic.ac.cn (Z. Wen).

0925-8388/$ – see front matter © 2010 Elsevier B.V. All rights reserved.
doi:10.1016/j.jallcom.2010.06.199

improving the cycling performances of silicon-based anodes. Li et al. [16] prepared a $FeSi_6$/graphite composite by mechanical ball milling, and the composite anode offers a large reversible capacity (about 800 mAh g^{-1}) and good cyclability. Alloys of Ti–Si and Ti–Si–Al were investigated as anode materials for lithium-ion batteries by Lee et al. [20]. It was shown that a critical milling time is required to attain good cycling performance. The $Ti_{28}Si_{72}$ alloy showing good cycling stability with small capacity, the partial substitution of Ti with Al could enhance the reversible capacity with comparable cycle performance.

In this work, we synthesized a novel Si–Ti alloy based composite using high energy mechanical milling (HEMM) followed by thermal treatment. In the composite, the nanosized Si, Ti and Si–Ti interphase alloy were uniformly distributed into an elastic glassy matrix to overcome the detriment of silicon anode. Ti is a good electron conductor that can alloy with Si during HEMM process. The Si–Ti alloys may not only improve the conductivity of the silicon active host but also can act as buffering matrices for the volume changes of Li–Si reaction. In addition, an elastic glassy matrix based on amorphous P_2O_5 and B_2O_3 can be in situ formed to effectively alleviate the volume changes of Si during cycling.

2. Experimental

Silicon (S) powder and titanium (T) powder (the mole ratio of Si to Ti was 2:1) with 2 wt.% of stearic acid as the dispersant were transferred into an 80 ml of steel vial in an argon-filled glove box (Korea Kiyon). Then the steel vial was sealed and transferred out of the glove box for high energy mechanical milling (HEMM). The HEMM was carried out in a mill of high frequency vibration and high speed centrifugal rotation (GN-2, Shenyang New Technology Scientific Instruments Co., Ltd.) at a rotation rate of 475 rpm. The mass ratio of milling balls to the reactants was 15:1. After 10 h of milling, 5 wt.% of B_2O_3 (B), 5 wt.% of P_2O_5 (P) and 10 wt.% of graphite (G) were added and further milled for 5 h. The as-milled powder was heated at 700 °C under vacuum for 3 h, and the final product was obtained without any grinding and sieving. The composite was marked as ST + GBP.

In order to make a comparison, another two samples were prepared: (1) silicon powder, titanium powder (same ratio as ST + GBP) and 20 wt.% of graphite (the amount of graphite was equal to the total amount of (graphite + B_2O_3 + P_2O_5) in ST + GBP) were milled together for 10 h and then the milled powder was heated at 700 °C under vacuum for 3 h. The final product was marked as STG; (2) silicon powder, 21 wt.% of graphite (the amount of graphite was equal to the total amount of (graphite + Ti) in ST + GBP), 5 wt.% of B_2O_3 and 5 wt.% of P_2O_5 were milled together for 10 h and heated under the same conditions. This sample was marked as SGBP.

The samples were characterized by X-ray diffraction (XRD, Rigaku RINT-2000) with Cu K_α radiation to identify the phases formed. Field emission scanning electron microscope (FESEM, JSM-6700F) and transmission electron microscope (TEM, JEM-2010) were applied to observe the morphology and particle size of the synthesized composite materials.

Electrodes containing 60 wt.% of the active materials (the as-prepared composite), 20 wt.% of polyvinylidene fluoride (PVDF) binder and 20 wt.% of carbon black were made by coating the slurry of the electrode ingredients in *N*-methyl pyrrolidinone (NMP) onto copper foil and dried at 100 °C under vacuum for 10 h. The thickness of the electrodes was about 28 μm. The working electrodes were assembled in 2025 coin cells using Celgard 2400 as the separator and lithium foils as the counter and reference electrodes. A solution of 1 M $LiPF_6$ in EC:DMC (1:1 weight) was employed as the electrolyte. The assembly of cells was processed in an argon-filled glove box with oxygen and water contents less than 1 ppm. The galvanostatic charge/discharge tests were conducted on a LAND CT2001A battery test system (Wuhan Land Electronics Co., Ltd., China) in voltage ranges of 0.02–1.5 and 0.05–1.0 V (vs. Li/Li^+) at a current density of 0.1 mA cm^{-2}. The electrochemical impedance spectroscopy (EIS) measurement has been conducted on an AUT83603 Electrochemical Workstation (Autolab Instruments, Netherlands) in the frequency range of 10^{-1}–10^5 Hz with alternating amplitude of 5 mV.

3. Results and discussion

3.1. Phase analysis

Fig. 1 shows the X-ray diffraction patterns of the as-prepared ST + GBP before and after heat treatment. As seen in Fig. 1(a), the ST + GBP composite before heat treatment consisted of Si, Ti, $TiSi_2$ and Fe (impurity). The diffraction peaks of Si and Ti is very strong, while the peak density of $TiSi_2$ alloy is very weak. After heat treatment, the peak density of Si became weak and the peaks of Ti_5Si_3 and TiSi appeared instead of Ti and $TiSi_2$, meaning that heat treatment contributed to the formation of Si–Ti alloys. In addition, the peak of FeC as an impurity was also observed and no SiC phase was observed by XRD patterns after heat treatment. The composition of B_2O_3, P_2O_5 and graphite were not observed for their amorphous structure.

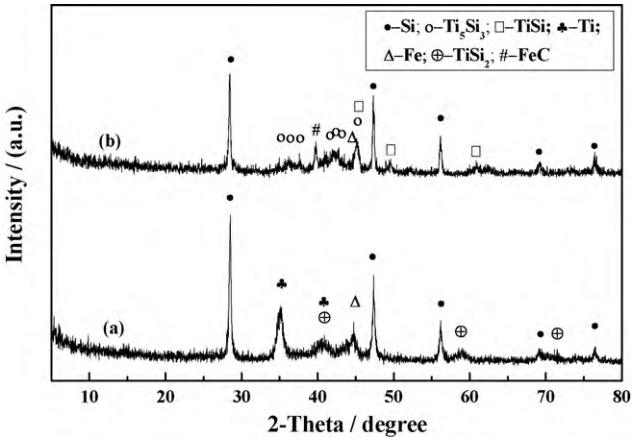

Fig. 1. X-ray diffraction patterns of the as-prepared ST + GBP composite powders: (a) before heat treatment and (b) after heat treatment.

3.2. Morphological feature

Fig. 2 shows the SEM morphology of the ST + GBP composite before (a) and after (b) heat treatment. As shown, the composite powders consisted of clusters with size of about hundreds of nanometers, while its primary particle size was only about dozens of to a hundred nanometers. Compared Fig. 2(a) with (b), it was concluded that heat treatment slightly increased the size of clusters due to particles agglomeration.

In order to observe the primary particle of the composite and to further confirm its phases, the transmission electron microscope (TEM) with X-ray energy-dispersive spectrometry (XEDS) was conducted and the results were shown in Fig. 3. In the TEM image of Fig. 3(a), the size of the primary particle was about 100 nm which was consistent with the SEM result. It was clear that the composite particle was covered by an amorphous gray layer with thickness of about 8–10 nm, where graphite is the predominant phase and the content of Si, Ti was relatively low, as shown in Fig. 3(b). While inside of the composite particle, it showed a homogenous dark appearance and mainly consisted of Si, Ti and C, as shown in Fig. 3(c). The content of O in both Fig. 3(b) and (c) was almost the same, meaning a uniform distribution of the amorphous oxides matrix in the whole composite.

3.3. Cycling performance

Fig. 4(a) and Table 1 show the cycling performance of the as-prepared two composite electrodes and the pure Si electrode in the voltage range of 0.02–1.5 V (vs. Li^+/Li) at the current density of 0.1 mA cm^{-2}. As seen, the pure Si electrode showed the largest reversible capacity among the three electrodes due to its high content of Si. And its initial coulombic efficiency was also higher than the composite electrodes, which might be due to its relatively large particle size (about 76 μm for the pure silicon and about 100 nm for the composite). However, in the 2nd cycle, the coulombic efficiency was only 67% and its cycling stability was very poor. After 50 cycles, the reversible capacity loss was up to 99%. For the ST + GBP composite electrode, although the 1st coulombic efficiency was

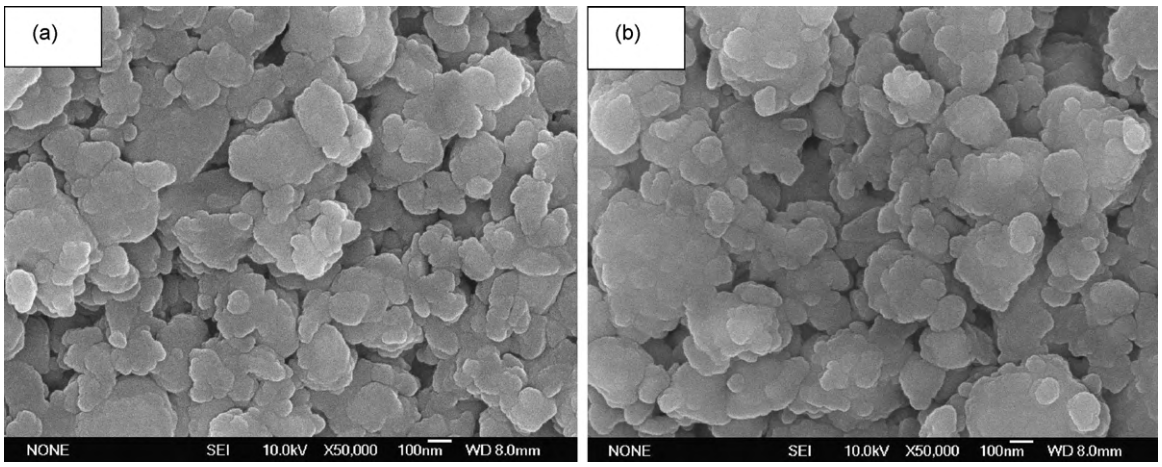

Fig. 2. SEM morphology of the as-prepared ST + GBP composite: (a) before heat treatment and (b) after heat treatment.

low, it revealed a much better cycling stability than those of the pure Si and the STG composite electrodes. From the 2nd cycle, the coulombic efficiency was up to 95% and a rechargeable capacity of 443.7 mAh g^{-1} was maintained after 50 cycles. It was concluded that, the uniform distribution of the active particles in the inactive amorphous matrix and the conductive graphite layer in and around the composite particles contributed to the improved cycling performance. Meanwhile, the pre-milling of Si and Ti as well as the

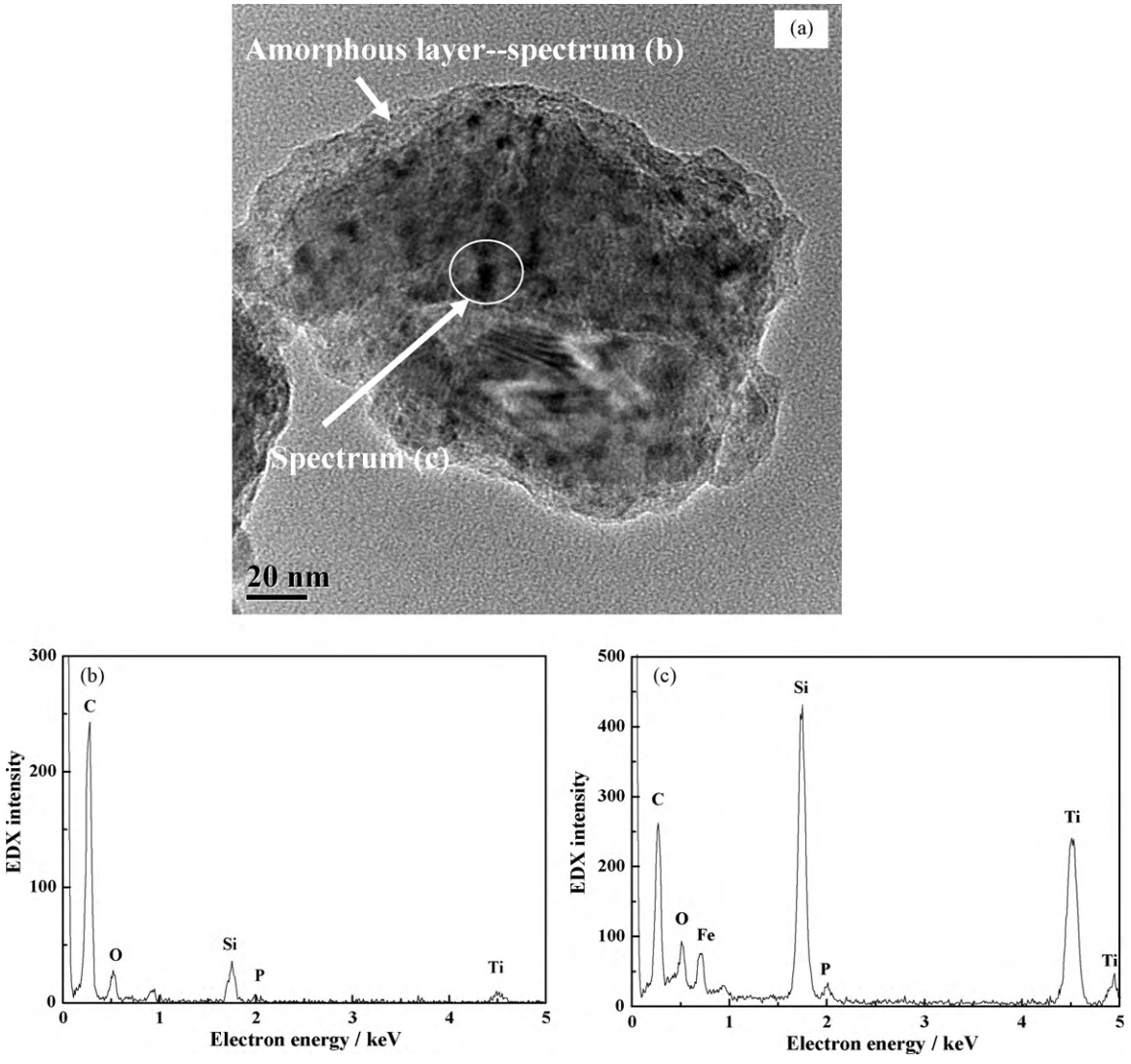

Fig. 3. (a) TEM image of the ST + GBP composite powder; (b) and (c) EDS spectra of the marked area in (a).

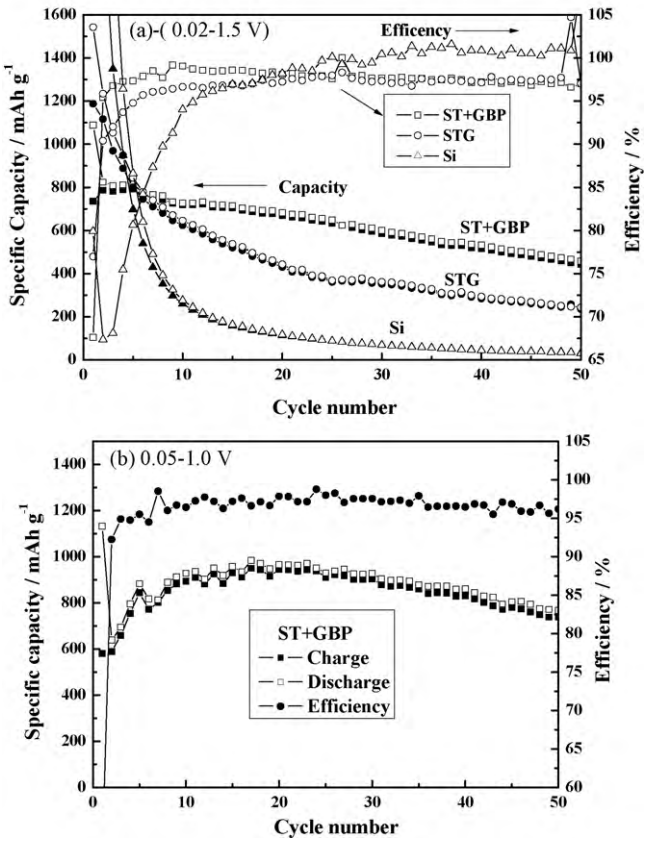

Fig. 4. Cycling performance for the as-prepared composite electrodes and the pure Si electrode at 0.1 mA cm^{-2} in the potential window of (a) 0.02–1.5 V and (b) 0.05–1.0 V.

heat treatment process were beneficial for the formation of certain amount of Si–Ti alloys which also contributed to the cycling stability.

The low initial coulombic efficiency of the ST + GBP composite electrode might be ascribed to the following factors: (1) the large surface area of the nanosized particles might lead to much more capacity loss on the formation of the solid electrolyte interface (SEI) films; (2) the high proportion of the binder and conducting black in the electrode might lower the coulombic efficiency; (3) the introduction of amorphous oxides (B_2O_3, P_2O_5) during HEMM process might cause the formation of some silica or titanic or other hanging bonds which would "capture" some Li^+ ions irreversibly during the 1st cycle. However, no peak corresponding to silica or titanic was found in the XRD patterns and further investigation still needed to be done.

Fig. 4(b) shows the cycling performance of the as-prepared ST + GBP composite electrode in the voltage range of 0.05–1.0 V (vs. Li^+/Li) at the current density of 0.1 mA cm^{-2}. As seen, the composite delivered a reversible capacity 581 mAh g^{-1} in the 1st cycle and after 50 cycles the reversible capacity was still up to 738.6 mAh g^{-1}, indicating that a slight increase of the discharge potential could effectively improve the cycling performance of the composite. The narrow voltage range can give better cycling stability than the relatively wide range for the lithium insertion/extraction is not completed, and thus gives small volume expansion [4].

Fig. 5 shows the cycling performance of the as-prepared composite electrode with discharge (lithium insertion) capacity limited to (a) 900 mAh g^{-1}, (b) 800 mAh g^{-1} and (c) 700 mAh g^{-1}, separately. If discharge capacity was limited to 900 mAh g^{-1}, during the 2nd cycle, the testing cell was overcharged. When discharged to 800 mAh g^{-1}, overcharging appeared at the 6th cycle. While discharged at 700 mAh g^{-1}, it delivered a reversible capacity of 675.8 mAh g^{-1} without any overcharging, and the coulombic efficiency remained over 95% from the 3rd cycle, showing a much better cycling performance than the literature [20].

Table 2
Values obtained from simulation of the ST + BPG, SGBP and Si electrodes.

Sample	R_1 (Ω)	R_2 (Ω)
ST + BPG	1.76	62.83
SGBP	3.32	90.94
Si	4.37	160.38

3.4. Electrochemical impedance spectroscopy

To further understand the reason for the improved cyclability of the composite electrode, electrochemical impedance spectroscopy (EIS) measurement has been conducted. Fig. 6 shows the comparison of the EIS spectra of the as-prepared ST + GBP, SGBP and the pure Si electrodes before cycling. The depressed semicircles in high frequency mainly correspond to the intrinsic electronic resistance and contact resistance of the composite electrode, as well as the passivated film on the lithium metal surface [25–27], indicating a better electronic conductivity and smaller contact resistance of the as-prepared ST + GBP composite electrode than those of the SGBP and Si electrodes. This was probably due to the good conduction network formed by Ti, Si–Ti alloy and graphite, as well as the homogenous distribution of the active Si particles in the conductive and amorphous matrix. Besides, in low frequency, the spectrum of the pure Si electrode displayed the behaviour of blocking electrode, while for the composite electrodes (ST + GBP and SGBP), the spectrum in the low frequency showed a declined line with a slope closed to 45°, representing the diffusion impedance of lithium ions in the composite (Warburg effect) [25,27]. This might be due to amorphous layer on the surface of Si particles.

The equivalent circuit is used to fit the EIS spectra of the composite (ST + GBP and SGBP) electrodes, as shown in Fig. 7. R_1 is the uncompensated ohmic resistance. The constant-phase element (CPE) corresponds to the dispersion effect. R_2 is related to the intrinsic electronic resistance and contact resistance of the composite electrode, as well as the passivated film on the lithium metal surface. W is related to the diffusion impedance (Wurburg impedance). The values obtained from simulation of the elements in equivalent circuit are shown in Table 2. The simulation is well consistent with the EIS spectra in Fig. 6.

Table 1
Comparison of the cycling performance for the ST + BPG, STG and Si electrodes.

Sample	1st charge (mAh g^{-1})	1st discharge (mAh g^{-1})	Efficiency (%)		50th charge (mAh g^{-1})	$R^*_{50/1}$ (%)
			1st	2nd		
ST + GBP	735.9	1088.4	68	95	443.7	60
STG	1187.2	1542	77	90	235.9	21
Si	3011.5	3768.1	80	67	32.7	1

$R^*_{50/1}$ – reversible capacity retention for the 50th cycle compared with the 1st cycle.

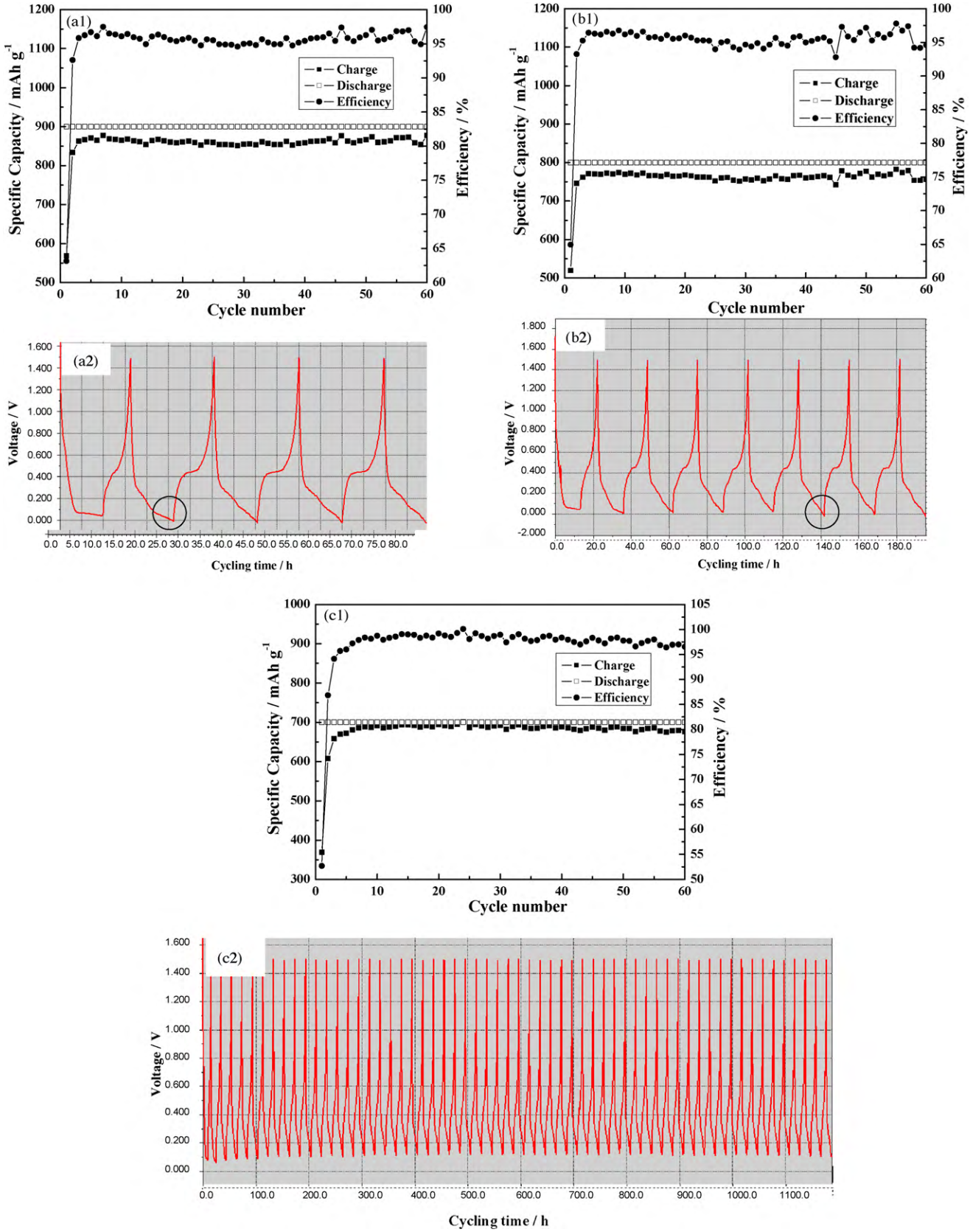

Fig. 5. Cycling performance of the as-prepared ST + GBP composite electrode with the discharge capacity limited to (a) 900 mAh g^{-1}, (b) 800 mAh g^{-1} and (c) 700 mAh g^{-1}; "1" – capacity vs. cycling number, "2" – charge/discharge voltage vs. cycling time.

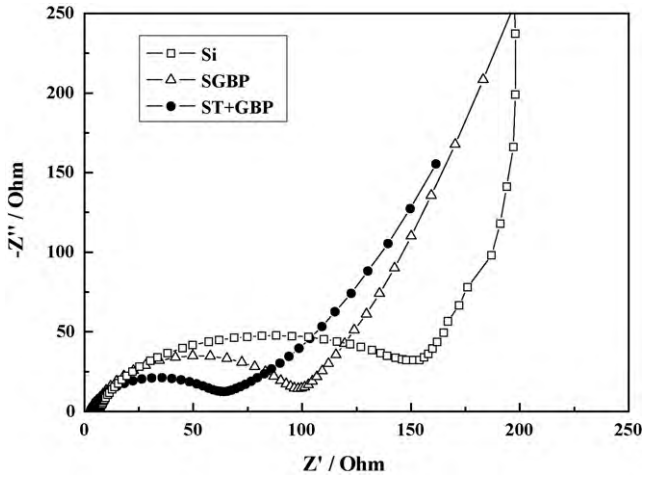

Fig. 6. Electrochemical impedance spectra of the ST + GBP composite, the SGBP and the pure Si electrodes.

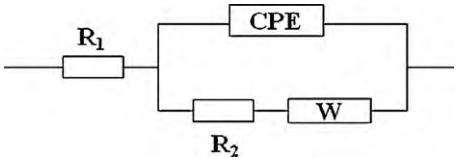

Fig. 7. Equivalent circuit of the composite electrodes.

4. Conclusions

A nanosized composite consisting of Si, Si–Ti alloy phases dispersed in a conductive graphite and inactive glassy matrix was prepared by HEMM followed by heat treatment. The composite delivered a reversible capacity of 738.6 mAh g^{-1} after 50 cycles and the coulombic efficiency remained over 95% from the 3rd cycle. When the discharge capacity was limited to 700 mAh g^{-1}, the reversible capacity was maintained at 675.8 mAh g^{-1} for 60 cycles without overcharge, showing a much better cycling performance than the pure Si electrode. It was concluded the uniform distribution of the active particles in the inactive amorphous matrix and the conductive graphite layer in and around the composite particles contributed to the improved cycling performance. In addition, the formation of certain amount of Si–Ti alloys was also benefit for the cycling stability.

Acknowledgments

This work was financially supported by NSFC Project Nos. 20333040 and 50672114, 863 Project of China No. 2006AA03Z232 and 973 Project of China No. 2007CB209700, as well as Research Projects from the Science and Technology Commission of Shanghai Municipality No. 08DZ2210900.

References

[1] W.J. Weydanz, M. Wohlfahrt-Mehrens, R.A. Huggins, J. Power Sources 81–82 (1999) 237.
[2] H. Li, X.J. Huang, L.Q. Chen, Z.G. Wu, Y. Liang, Electrochem. Solid-State Lett. 2 (1999) 547.
[3] J. Graetz, C.C. Ahn, R. Yazami, B. Fultz, Electrochem. Solid-State Lett. 6 (2003) A194.
[4] M.K. Datta, P.N. Kumta, J. Power Sources 194 (2009) 1043.
[5] Q. Si, K. Hanai, T. Ichikawa, A. Hirano, N. Imanishi, Y. Takeda, O. Yamamoto, J. Power Sources 195 (2010) 1720.
[6] Y. Eker, K. Kierzek, E. Raymundo-Pinero, J. Machnikowski, F. Béguin, Electrochim. Acta 55 (2010) 729.
[7] Y.N. Jo, Y. Kim, J.S. Kim, J.H. Song, K.J. Kim, C.Y. Kwag, D.J. Lee, C.W. Park, Y.J. Kim, J. Power Sources 195 (2010) 6031.
[8] P. Gu, R. Cai, Y. Zhou, Z. Shao, Electrochim. Acta 55 (2010) 3876.
[9] Z. Zhou, Y. Xu, W. Liu, L. Niu, J. Alloys Compd. 493 (2010) 636.
[10] G.X. Wang, L. Sun, D.H. Bradhurst, S. Zhong, S.X. Dou, H.K. Liu, J. Alloys Compd. 306 (2000) 249.
[11] M.-S. Park, Y.-J. Lee, S. Rajendran, M.-S. Song, H.-S. Kim, J.-Y. Lee, Electrochim. Acta 50 (2005) 5561.
[12] M.-S. Park, Y.-J. Lee, S. Rajendran, M.-S. Song, H.-S. Kim, J.-Y. Lee, J. Power Sources 158 (2006) 650.
[13] J.W. Kim, J.H. Ryu, K.T. Lee, S.M. Oh, J. Power Sources 147 (2005) 227.
[14] K. Wang, X.M. He, L. Wang, J.G. Ren, C.Y. Jiang, C.R. Wan, Solid State Ionics 178 (2007) 115.
[15] P.J. Zuo, G.P. Yin, X.F. Hao, Z.L. Yang, Y.L. Ma, Z.G. Gao, Mater. Chem. Phys. 104 (2007) 444.
[16] T. Li, Y.L. Cao, X.P. Ai, H.X. Yang, J. Power Sources 184 (2008) 473.
[17] H. Dong, X.P. Ai, H.X. Yang, Electrochem. Commun. 5 (2003) 952.
[18] C.-H. Doh, H.-M. Shin, D.-H. Kim, Y.-D. Jeong, S.-I. Moon, B.-S. Jin, H.-S. Kim, K.-W. Kim, D.-H. Oh, A. Veluchamy, J. Alloys Compd. 461 (2008) 321.
[19] Y.-S. Lee, J.-H. Lee, Y.-W. Kim, Y.-K. Sun, S.-M. Lee, Electrochim. Acta 52 (2006) 1523.
[20] K.-M. Lee, Y.-S. Lee, Y.-W. Kim, Y.-K. Sun, S.-M. Lee, J. Alloys Compd. 472 (2009) 461.
[21] Z.B. Sun, X.D. Wang, X.P. Li, M.S. Zhao, Y. Li, Y.M. Zhu, X.P. Song, J. Power Sources 182 (2008) 353.
[22] M. Li, Z. Yu, X. He, Electrochim. Acta 55 (2010) 2217.
[23] M. Li, Z. Yu, M. Qu, J. Alloys Compd. 491 (2010) 643.
[24] Z.W. Lu, G. Wang, X.P. Gao, X.J. Liu, J.Q. Wang, J. Power Sources 189 (2009) 832.
[25] J.Y. Song, H.H. Lee, Y.Y. Wang, C.C. Wan, J. Power Sources 111 (2002) 255.
[26] T. Jiang, S. Zhang, X. Qiu, W. Zhu, L. Chen, Electrochem. Commun. 9 (2007) 930.
[27] N. Dimov, S. Kugino, M. Yoshio, Electrochim. Acta 48 (2003) 1579.